THE JOURNAL OF PHYSICAL CHEMISTRY B

Article

pubs.acs.org/JPCB

Molecular Dynamics Study of Ionic Liquids Complexation within β-Cyclodextrins

Rocío Semino[†] and Javier Rodríguez*[,‡,§]

[†]Departamento de Química Inorgánica, Analítica y Química Física, Facultad de Ciencias Exactas y Naturales, Universidad de Buenos Aires, Pabellón II, Ciudad Universitaria (1428) Capital Federal, Argentina

[‡]Departmento de Física de la Materia Condensada, Comisión Nacional de Energía Atómica, Avenida Gral. Paz 1499 (1650) San Martín, Provincia de Buenos Aires, Argentina

[§]ECyT, UNSAM, Martín de Irigoyen 3100 (1650) San Martín, Provincia de Buenos Aires, Argentina

ABSTRACT: We have studied 1:1 inclusion complexes of two imidazole-based ionic liquids within β-cyclodextrin: 1-dodecyl-3-methylimidazolium and 1-butyl-3-methylimidazolium. By means of an adaptive biasing force scheme, we obtained the free energy profile along two different pathways, differing in the orientations of the head-to-tail vector with respect to the primary−secondary rim axis. Regarding 1-dodecyl-3-methylimidazolium, we found one minimum energy structure for each pathway, in which the hydrophobic tail remains embedded within the cyclodextrin, while the headgroup lies ∼11−12 Å from one of the rims; the structure where the polar head lies near the primary rim is the more stable. The analysis of the free energy of encapsulation of 1-butyl-3-methylimidazolium shows two minima for each insertion pathway, each of them associated with configurations where the imidazolium head lies close to one of the polar rims. As such, the most stable structure corresponds to one where the hydrophobic tail lies embedded within the cyclodextrin, while its head is localized near the secondary rim. The results are interpreted in terms of a simple model which captures the essential features that control the encapsulation process. A comparison with available experimental data is presented.

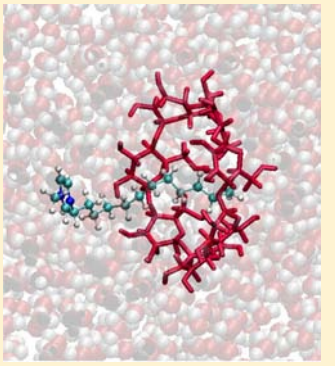

1. INTRODUCTION

Cyclodextrins (CD) are cyclic oligosaccharides composed of six (α-CD), seven (β-CD), or eight (γ-CD) glucose units,[1] linked together by 1,4 glycosidic bonds. Their overall molecular shape is that of a truncated cone, with an hydrophobic cavity and a polar surface, characterized by hydroxylated, hydrophilic rims (a narrower, primary rim and a wider, secondary rim). This particular geometry gives CDs a highly versatile ability to form inclusion complexes with different kinds of organic solutes, a fact that makes them useful in food industry,[2] as drug carriers,[3−6] as building blocks for polymers,[7,8] and as adsorbents for separation techniques,[9] to cite a few relevant applications.

On the other hand, in the past decade, room temperature ionic liquids (RTILs) have attracted considerable attention as possible replacements for organic solvents, because they are nonvolatile, nonflammable, thermally and chemically stable, highly polar, and environmentally friendly.[10] These molten organic salts have been used together with CDs in a wide range of applications, such as in enantioseparation by electrophoresis,[11−14] in gas and high-performance liquid chromatographies,[15,16] and also in supramolecular chemistry, for the synthesis of new materials with many interesting properties, including polyrotaxanes and polypseudorotaxanes.[17−22] In all these fields, the knowledge of the characteristics of CD−RTIL interactions is of major interest.

Several experimental works have been devoted to systems combining RTILs and CDs. From the structural point of view, Gao et al. studied the encapsulation of 1-butyl-3-methylimidazolium (C_4mim^+) and 1-dodecyl-3-methylimidazolium ($C_{12}mim^+$) in β-CD relying on ^1H NMR, among other techniques.[23,24] In their work, the authors proposed different structures for 1:1 inclusion complexes. For the larger RTIL, two possible configurations are described, each of them involving the inclusion of a portion of the hydrophobic tail inside the nonpolar cavity of β-CD, while the polar head remains immersed in the bulk solvent.[24] The difference between these structures resides in the fact that the imidazolium head can rest closer either to the primary or to the secondary rim. Contrasting, for the shorter RTIL, the authors proposed only one structure, where the RTIL is completely embedded within the β-CD cavity, with its head pointing toward the primary rim.[23] From a binding equilibrium perspective, many works have been devoted to the analysis and comparison of different complexation constants.[25−29] Yet many aspects related to the sources of the stabilization and the microscopic characteristics of the RTIL−CD association still remain to be unveiled. In what follows, we will present a microscopic description of the association between β-CD and two imidazolium-based RTILs with different hydrophobic tail lengths, relying on molecular dynamics (MD) simulations and free-energy calculations. The MD approach has been successfully implemented to analyze

Received: January 28, 2015
Revised: March 13, 2015

DOI: 10.1021/acs.jpcb.5b00909
J. Phys. Chem. B XXXX, XXX, XXX−XXX

solvation of a large variety of host−CD complexes in vacuo and in solution. Reference 30 provides a comprehensive review article about this issue.

The organization of this paper is as follows: in section 2 we describe the system and the molecular dynamics simulations performed, section 3 includes the results of our simulation experiments, and section 4 contains the discussion of these results. Finally, in section 5 we summarize the most relevant results of this paper.

2. SYSTEMS STUDIED AND SIMULATION DETAILS

We performed molecular dynamics experiments on aqueous solutions containing a single β-CD and an infinitely diluted imidazole-based cation. Two systems, differing in the hydrophobicity of the charged solute, were analyzed: the first one corresponded to 1-dodecyl-3-methylimidazolium, whereas the second one corresponded to 1-butyl-3-methylimidazolium (see Figure 1). These molecules are typical cationic species of RTIL,

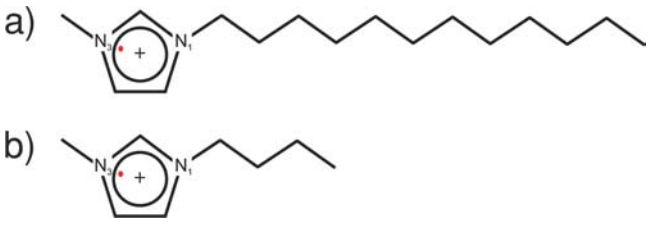

Figure 1. Chemical structures of the RTILs investigated: (a) 1-dodecyl-3-methylimidazolium; (b) 1-butyl-3-methylimidazolium. The red dots indicate the positions of the centers of mass of the imidazolium heads.

and structurally speaking, both can be portrayed in terms of an ionic imidazolium headgroup attached to hydrophobic tails of different lengths.

In the two cases, the systems comprised N_w = 1654 water molecules, confined within a rectangular box with linear dimensions close to 30 Å × 30 Å × 60 Å. The dynamical trajectories corresponded to isobaric−isothermal (NPT) simulation runs implemented via a Langevin dynamics, that maintained the pressure and temperature at the vicinity of 1 bar and T = 298 K, respectively. The trajectories were generated using the NAMD package,[31] with interactions taken from the CHARMM22 force field.[32] Parameters for intra- and intermolecular interactions involving sites in the ionic liquid cation were taken from ref 33, whereas water interactions were modeled using the classical TIP3P model.[34] These Hamiltonians have been employed in previous studies dealing with similar types of systems.[35−38] Long ranged Coulomb forces were treated using standard Ewald sums, assuming the presence of a continuous neutralizing background.

Coordinates of the β-CD were obtained from neutron diffraction information.[39] In all simulation experiments, the initial orientation of the CD was chosen so as to make the primary rim−secondary rim vector parallel to the longest axis of the simulation box (hereafter referred to as the z-axis). Two insertion paths, $\mathcal{A}$ and $\mathcal{B}$ (see Figure 2), differing in the orientations of the head-to-tail vector with respect to the z-axis, were considered. In all cases, the initial intramolecular configurations of the alkyl chains in the RTIL corresponded to fully trans conformers. Finally, the systems were filled up with water molecules and equilibrated for about 200 ps, in a run in which only the solvent molecules were allowed to move, at

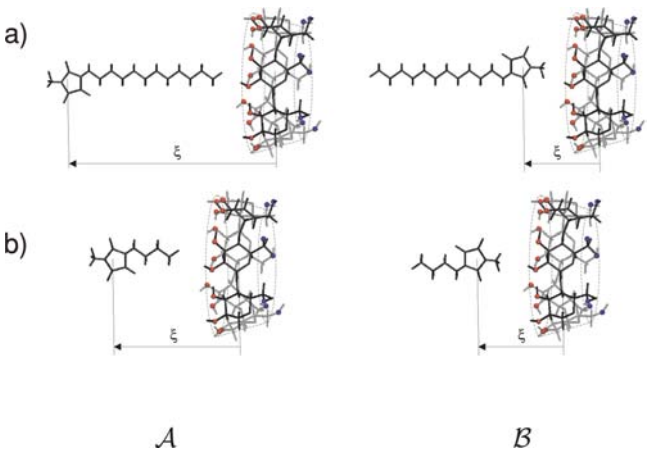

Figure 2. Insertion pathways of RTIL's cation within β-CD: (a) 1-dodecyl-3-methylimidazolium; (b) 1-butyl-3-methylimidazolium. For the sake of clarity oxygen atoms corresponding to the primary and secondary hydroxyl groups of the CD are rendered in blue and red, respectively.

temperatures close to T = 700 K. From then on, the systems were gradually cooled down to temperatures close to ambient conditions, by multiple rescalings of the atomic velocities during a time interval of 100 ps. During this period, we released the initial constraints on the cation and on the CD sites, with the exception of six spherically symmetric, soft harmonic interactions with restoring force constants $k_{rst} \sim 15$ kcal mol^{-1} Å^{-2},[40] acting on each glycosidic oxygen site that avoided global modifications of the initial orientation. In all cases, we verified that this external potential introduced only minor modifications to the overall dynamics along the insertion channels.

3. RESULTS

In order to describe the different stages of the insertion process of the RTIL cation within the CD cavity, we found it convenient to adopt a simple geometrical order parameter ξ, defined as

$$\xi = Z_{IL} - Z_{CD} \quad (1)$$

In eq 1, Z_{CD} and Z_{IL} correspond to the z-coordinates of the centers of mass of the β-CD and the RTIL imidazolium group, which is located nearby the position of the N_3 atom, slightly shifted inward the ring (see also Figure 2). Associated with this order parameter there is a corresponding Gibbs free energy defined in terms of

$$-\beta G(\xi^\circ) \propto \ln\langle\delta(\xi - \xi^\circ)\rangle \quad (2)$$

where the angular brackets denote an equilibrium ensemble average, δ corresponds to the delta-function centered at a given value of the reaction coordinate, ξ°, and $\beta = (k_B T)^{-1}$ corresponds to the inverse of the temperature times the Boltzmann constant.

In Figure 3 we present results for $\Delta G(\xi) = G(\xi) - G(\xi = \infty)$. In all cases, the curves were obtained implementing an adaptive biasing forces (ABF) protocol.[41−43] The latter methodology has been successfully employed in analysis of encapsulation processes involving a large variety of guest molecules in CDs, ranging from simple ionic species[35] up to much more complex guests such as steroids,[44] rotaxanes,[45] cholesterol,[46] and Amphotericin B.[47] The basic idea behind this scheme relies on the generation of trajectories along a chosen

DOI: 10.1021/acs.jpcb.5b00909
J. Phys. Chem. B XXXX, XXX, XXX−XXX

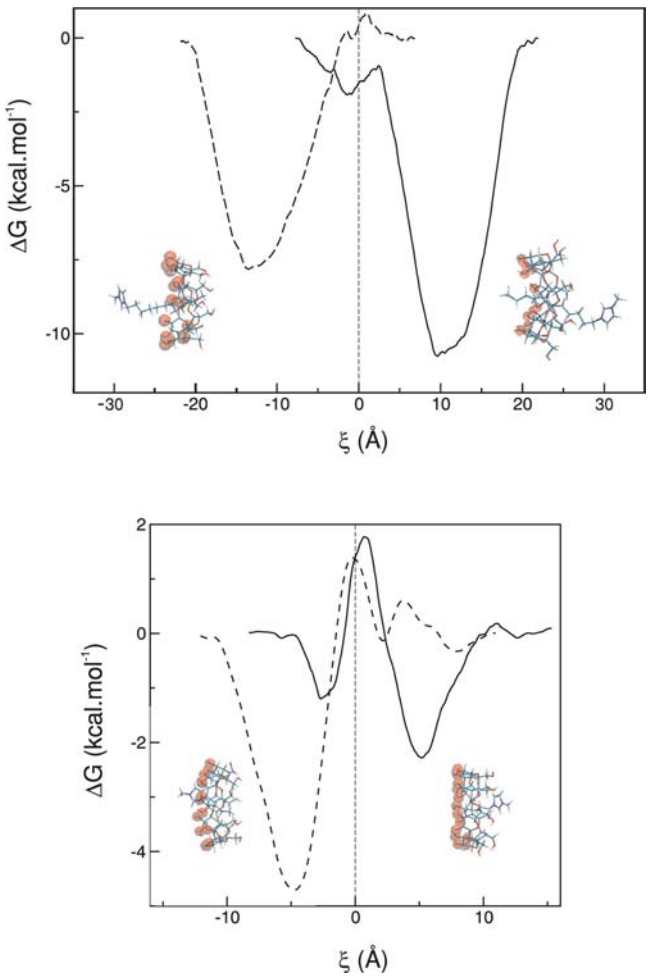

Figure 3. Gibbs free energy profiles for the inclusion of RTIL cation within an β-CD. Top panel, 1-dodecyl-3-methylimidazolium; bottom panel, 1-butyl-3-methylimidazolium. The dashed and solid lines correspond to the $\mathcal{A}$ and $\mathcal{B}$ insertion pathways, respectively. Typical snapshots of the inclusion complexes at the minimum energy configurations for both insertion pathways are displayed.

reaction coordinate, experiencing practically no free energy barriers. This is achieved by estimating biasing forces along a series of bins, spanning the complete ξ interval. These forces flatten the free energy surface, so that the reaction coordinate becomes uniformly sampled. Our procedure to implement the algorithm involved the following: (i) we first divided the relevant portion of the insertion path interval -20 Å $\lesssim \xi \lesssim 20$ Å into 20 overlapping windows; (ii) confining potentials along the x and y directions (harmonic constant $k_{x-y} \sim 0.5$ kcal mol^{-1} Å^{-2}) acting on the N_3 site of the imidazolium ring and on the terminal C atom of the methyl group in the longest aliphatic tail were also applied. In doing so, we preserved the initial overall intramolecular geometry of the cation, at large values of ξ, and, incidentally, restricted the sampling over the $\rho^2 = x^2 + y^2 \lesssim 25$ Å^2 cylindrical region. Within each window, instantaneous values of the forces were collected in bins 0.1 Å wide. The sampling within each window required typically $\sim 2 \times 10^6$ simulation steps to attain proper convergence.

The free energy profiles are shown in the top ($C_{12}mim^+$) and bottom (C_4mim^+) panels of Figure 3. Concerning the profiles for $C_{12}mim^+$, two important observations are to be noted: (i) the magnitudes and (ii) the symmetry of the positions of the corresponding global minima with respect to the full encapsulation of the headgroup, $\xi = 0$. Our simulations show that the most stable configuration of the RTIL–CD complex corresponds to the insertion pathway $\mathcal{B}$, with $\Delta G(\xi \sim 11$ Å$) \sim -12$ kcal mol^{-1}. These values correspond to an arrangement in which the cation lies with a substantial portion of its hydrophobic tail embedded within the CD cavity, while the imidazolium group lies in a position somewhat external with respect to the CD primary rim. Similar geometrical characteristics are found in the solvation structure that prevails in the vicinity of the shallower global minimum along the path $\mathcal{A}$, $\Delta G(\xi \sim -12$ Å$) \sim -7.5$ kcal mol^{-1}, except that, along this channel, the headgroup lies at the vicinity of the other, secondary, rim. These two complex structures, in which the hydrophobic tail is embedded within the CD cavity and the imidazolium ring lies surrounded by the external solvent, are in close agreement with those proposed by Gao et al.[24]

At a first glance, the characteristics of the free energy profiles for cations with shorter alkyl tails shown in the bottom panel of Figure 3 look inverted while the magnitudes of the global minima are somewhat less pronounced. As a new feature, in both profiles, there is evidence of a local maximum near $\xi \sim 0$, flanked by two lateral minima. These minima correspond to configurations in which the headgroup of the RTIL lies close to one of the rims. For each insertion pathway, the most stable minimum is the one for which not only does the headgroup coincide with one of the polar rims, but also the hydrophobic tail lies embedded within the CD cavity. The secondary minima correspond to spatial arrangements where the headgroup of the RTIL interacts with the other rim of the CD, while its tail is surrounded by water molecules, disrupting the hydrogen bond network. In particular, for path $\mathcal{B}$, the difference between minima ($\Delta(\Delta G^{\mathcal{B}}_{min}) \sim 1$ kcal mol^{-1}) is small enough to conclude that both structures are comparable in terms of their relative stability. Finally, note that the stabilization energy of the RTIL–CD complex at the global minimum for path $\mathcal{A}$ (dashed line) is nearly 2 times larger than the corresponding one for path $\mathcal{B}$ (solid line), i.e., $\Delta G^{\mathcal{A}\to\mathcal{B}}_{min} \sim 2$ kcal mol^{-1}.

To conclude, we present an estimate of the free energy of encapsulation ΔG°_{enc}, which can be readily obtained by integrating the corresponding free energy profiles, namely

$$-\beta \Delta G^{\circ}_{enc} = \ln \frac{\pi N_A \int_{-\infty}^{\infty} r_{av}{}^2(\xi) \exp[-\beta \Delta G(\xi)]\, d\xi}{dm^3} \quad (3)$$

where r^2_{av} is the ξ-dependent average ratio of the cross section of β-CD, and N_A is Avogadro's number. Results for ΔG°_{enc} are listed in Table 1, along with available experimental information. Note that our simulation results feature two values of ΔG°_{enc}, one for each insertion pathway, while the experiments provide only one value, which contains contributions for the two possible orientations and, eventually, includes contributions derived from the anion complexation.

Table 1. Experimental and Calculated Encapsulation Free Energies Expressed in kcal mol^{-1}

	exptl ΔG°_{enc} [a]	calcd ΔG°_{enc}	
		$\mathcal{A}$	$\mathcal{B}$
C_4mim^+–β-CD	−1.3,[b] −2.0[c]	−2.8	−0.6
$C_{12}mim^+$–β-CD	−5.5[c]	−5.0	−8.7

[a]From ref 25. [b]Anion: Cl^-. [c]Anion: BF_4^-.

DOI: 10.1021/acs.jpcb.5b00909
J. Phys. Chem. B XXXX, XXX, XXX–XXX

Although our simulation results adequately reproduce the experimental trends, the calculated encapsulation energies are about ∼2−3 kcal mol^{-1} lower than the corresponding experimental ones. This difference can be mainly ascribed to the loss of configurational entropy in the calculation, due to the restrains imposed on the motion of the RTIL to ensure an appropriate sampling.[44] Note that our procedure does not include relevant rotational and translational degrees of freedom of the guest. This leads to an underestimation of ΔG°_{enc} values of $\sim RT \sim 0.5$ kcal mol $^{-1}$, since two rotational degrees of freedom are being ignored. Contributions from translational degrees of freedom are difficult to estimate. A conservative guess would be close to ∼1.5 kcal mol^{-1}.[48]

Other possible sources of the differences between experimental and theoretical values can be traced back to limitations in the parametrization of the force field and, furthermore, to the absence of anions in the simulation experiments (experimental results seem to be very sensitive to the type of anion of the ionic liquid: see for example the differences between ΔG°_{enc} for $C_4mim^+Cl^-$ and $C_4mim^+BF_4^-$ in Table 1).

Comparison of ΔG°_{enc} values between different RTILs shows an increment of the order of ∼2−10 times for this stabilization energy as the hydrophobic tail length increases. In section 4 we will present a detailed analysis of the characteristics of each RTIL−β-CD inclusion process, so as to assess the origin of the observed differences.

4. DISCUSSION

4.1. C_4mim^+. In order to gain additional insight into the encapsulation process of C_4mim^+ in a β-CD, we elaborated a simple model capable of capturing the essential features of the free energy profiles presented above.

The model combines the following ingredients:

1. The RTIL was modeled as two rigid spheres in contact, with radius r_o = 2.7 Å. The first one mimics the hydrophobic tail, whereas the second one—at the center of which a single positive charge (e) was located—represents the hydrophilic headgroup of the RTIL (see Figure 4a)). The volume of the model RTIL is $2V_{ctrl} = 2(4/3)\pi r_o^3 \sim 165$ Å^3, in close agreement with the calculated molecular volume of the probe.[49]

2. The interaction between the β-CD and the RTIL is represented exclusively by the Coulombic coupling between the host and the positive charge. To this end the Coulombic field generated by the β-CD along its cylindrical axis was calculated according to

$$V_{CD}(z) = \left\langle \sum_i^{N_{CD}} \frac{q_i}{x_i^2 + y_i^2 + (z - z_i^2)} \right\rangle \quad (4)$$

where N_{CD} is the total number of atomic sites of the host; q_i, x_i, y_i, and z_i correspond to the partial charge and the Cartesian coordinates of the ith site of the CD, respectively. The Coulombic potential was averaged over an ensemble of β-CD configurations, harvested along the ABF trajectories for the different pathways analyzed (see Figure 4b).

3. The aqueous solvent was represented by a continuous medium within which the RTIL−β-CD pair was immersed. The dielectric constant of water (ϵ_w) was considered to be a linear function of the water local density, according with available experimental data.[50] The latter was calculated according to

$$\rho_w(z) = \frac{1}{\pi R^2} \sum_i \langle \delta(z_i^w - Z_{CD} - z) \rangle_{cyl} \quad (5)$$

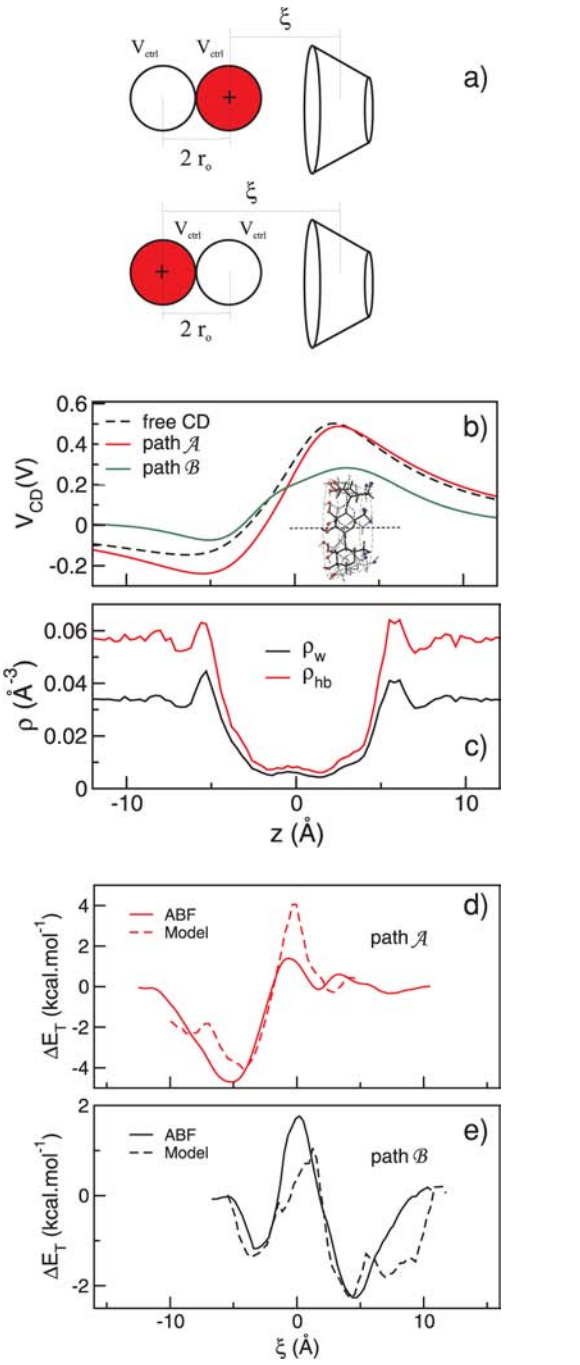

Figure 4. (a) Scheme of the model to study the encapsulation complexes of C_4mim^+ in a β-CD. The picture above represents $\mathcal{B}$ pathway, while the one below corresponds to $\mathcal{A}$ pathway. (b) V_{CD} for three different configurations: free CD (black, dashed line), pathway $\mathcal{A}$ CD (red, solid line), and pathway $\mathcal{B}$ CD (green, solid line). (c) Water and hydrogen bond densities as a function of the distance. (d, e) Energy profiles obtained by ABF techniques (solid lines) and by the application of our model (dashed lines) for $\mathcal{A}$ and $\mathcal{B}$ pathways, respectively.

In eq 5, $\langle ... \rangle_{cyl}$ denotes an equilibrium ensemble average, taken over a cylindrical region of the simulation box axially alligned to the cylindrical axis of the CD, with radius R = 8 Å; z_i^w represents the z-coordinate of the oxygen site of the ith water molecule (see Figure 4c).

4. There is also one more energy contribution left to be considered in the encapsulation process: the work involved in

DOI: 10.1021/acs.jpcb.5b00909
J. Phys. Chem. B XXXX, XXX, XXX−XXX

the creation of a cavity, mainly associated with the rearrangement of the hydrogen bond network required to accommodate the two spheres within the water. Note that solvent stabilizes as the RTIL moves from rich-to-low density regions. In our model, at a given ξ, the solvent−solvent interactions depend on the number of hydrogen bonds within the control volume. The hydrogen bond density (ρ_{hb}) is determined in a way similar to that described for the calculation of ρ_w, taking into account the hydrogen bond definition presented in ref 51 (see Figure 4c).

5. In order to compute the energy profiles, the probe was displaced along the cylindrical axis of the β-CD, and the potential energy, $E_T(\xi)$, was calculated as a sum of two contributions: (i) the Coulombic coupling between the charge and the CD, screened by the dielectric medium, namely

$$E_{coul}(z) = \frac{eV_{CD}(z)}{\epsilon_w(z)} \propto \frac{eV_{CD}(z)}{\rho_w(z)} \quad (6)$$

and (ii) the cavity contribution

$$E_{cavity}(z) \propto \rho_{hb}(z)V_{ctrl} \quad (7)$$

6. The resulting total energy is determined for pathway $\mathcal{A}$ by

$$E_T(\xi) = E_{coul}(\xi) + E_{cavity}(\xi) + E_{cavity}(\xi + 2r_o) \quad (8)$$

or, for pathway $\mathcal{B}$ by

$$E_T(\xi) = E_{coul}(\xi) + E_{cavity}(\xi) + E_{cavity}(\xi - 2r_o) \quad (9)$$

A graphical representation of the model is depicted in panel a of Figure 4.

A comparison of the results obtained from this model with the ABF potential energy curves for both encapsulation pathways is shown in panels d and e of Figure 4. Even though there are some minor differences in the positions and depths of the minima, our simplified model does reproduce the relevant features of the potential curves. The analysis of the different energetic contributions suggests that the secondary rim of the CD (negative electric potential region) interacts much more strongly with the positive charged cationic head than the primary rim does. This observation agrees with a previous study made in our group, in which anions were found to form encapsulation complexes near the primary rim of the CD (positive electric potential region).[35] As a consequence, the global minimum for the C_4mim^+−β-CD complex corresponds to configurations in which the hydrophobic tail lies within the hydrophobic CD cavity, whereas the RTIL headgroup remains in close contact with the secondary rim. Furthermore, one could speculate that the presence of a secondary minimum ($\xi \sim$ 3 Å) in pathway $\mathcal{B}$ would indicate that the coupling between the imidazolium head and the secondary CD rim is strong enough to compensate the unfavorable interaction between the hydrophobic tail and the water molecules.

At this point, it is worth commenting on the experimental results presented by Gao et al.[23] Based on the analysis of chemical shifts in the ^{1}H NMR spectra of the RTIL−β-CD complex, the authors have proposed a minimum energy inclusion moiety in which the RTIL headgroup lies in close contact with the CD primary ring. On the other hand, our calculations predict a most stable complex structure in which the guest molecule rests in an opposite orientation. The interpretation of the experimental signals made by Gao et al. is based on the assumption that the imidazolium ring enters the cavity of the β-CD from the secondary, wider, rim. Our calculations show no significative differences between the energy barriers associated with the different insertion pathways (see bottom panel in Figure 3). Consequently, it does not seem to be a preferential entrance channel for the RTIL. Beyond this fact, we tend to believe that the structure predicted by our calculations for the minimum is consistent with the experimental results: (i) first, H_3 and H_5 CD protons (located at the inner surface of cavity) should exhibit upfield shifts due to their interactions with both the headgroup and the aliphatic RTIL tail; (ii) contrasting, H_4 and H_5 imidazole ring proton signals should be downfield shifted due to their close interaction with the oxygen atoms at the secondary rim, and probably collapse into a single signal (analysis of radial distributions functions of the type O_2, O_3−H_4, H_5, not shown here, reveal equivalent environments for both atoms).

4.2. $C_{12}mim^+$. In section 3 we showed that there is a preferential stabilization of $C_{12}mim^+$ along pathway $\mathcal{B}$, with its hydrophobic tail embedded within the β-CD and its headgroup located ∼11 Å from the primary rim. Since the distances between the imidazolium head and the CD rims are longer than the ones found for the shorter RTIL, there is no evidence that the Coulombic coupling discussed in section 4.1 contributes to the stabilization of the complexes. As such, the encapsulation seems to be mainly driven by hydrophobic interactions. In the following paragraphs, we will show that the differences in the solvation of the OH groups located in the secondary rim of the CD will be the new relevant feature that might explain the stabilization of the $C_{12}mim^+$−β-CD moiety. To this end, a statistic of relevant observables was harvested along unconstrained trajectories, initially equilibrated at the vicinities of the different global minima of the $C_{12}mim^+$−CD complexes. Note that the depths of the relevant free energy wells (see Figure 3) are sufficiently large so as to make it possible to collect physically sound averages from unconstrained runs. In fact, we verified that the logarithms of the histograms for the reaction coordinate collected along these trajectories lasting typically ∼4−6 ns (not shown) do reproduce the free energy well profiles obtained from ABF trajectories.

In order to characterize the intramolecular hydrogen bonds in the CD, we calculated radial density profiles of the form

$$\rho_{O_\alpha HO_\beta}(r) = \frac{1}{4\pi r^2 N_i} \sum_i \sum_j \langle \delta(|\mathbf{r}_i^{O_\alpha} - \mathbf{r}_j^{HO_\beta}| - r) \rangle \quad (10)$$

In eq 10, $N_i = 7$, $\mathbf{r}_i^{O_\alpha}$ represents the coordinate of the ith α-oxygen site, and $\mathbf{r}_j^{HO_\beta}$ corresponds to the jth hydrogen bonded to a β-oxygen, both lying at the secondary rim of CD (see lower panel in Figure 5).

On the other hand, solvation at the secondary rim was described in terms of the following radial density function:

$$\rho_{O_\alpha H_w}(r) = \frac{1}{4\pi r^2 N_i} \sum_i \sum_j \langle \delta(|\mathbf{r}_i^{O_\alpha} - \mathbf{r}_j^{H_w}| - r) \rangle \quad (11)$$

where $\mathbf{r}_j^{H_w}$ corresponds to the jth water hydrogen site.

In Figure 5 we present plots for these spatial correlations. At a first glance, it is clear that the solvation structures for pathways $\mathcal{A}$ and $\mathcal{B}$ look markedly different. Most importantly, in the $\mathcal{B}$ profile, there is a peak located at $r \sim 1.95$ Å (more pronounced for $\rho_{O_2HO_3}$) that is absent in pathway $\mathcal{A}$. This peak is also featured in the hydrated β-CD system in the absence of RTIL (not shown), revealing the presence of intramolecular hydrogen bonding between adjacent glycosidic units. As such, along the $\mathcal{A}$ pathway, the presence of $C_{12}mim^+$ somehow alters

DOI: 10.1021/acs.jpcb.5b00909
J. Phys. Chem. B XXXX, XXX, XXX−XXX

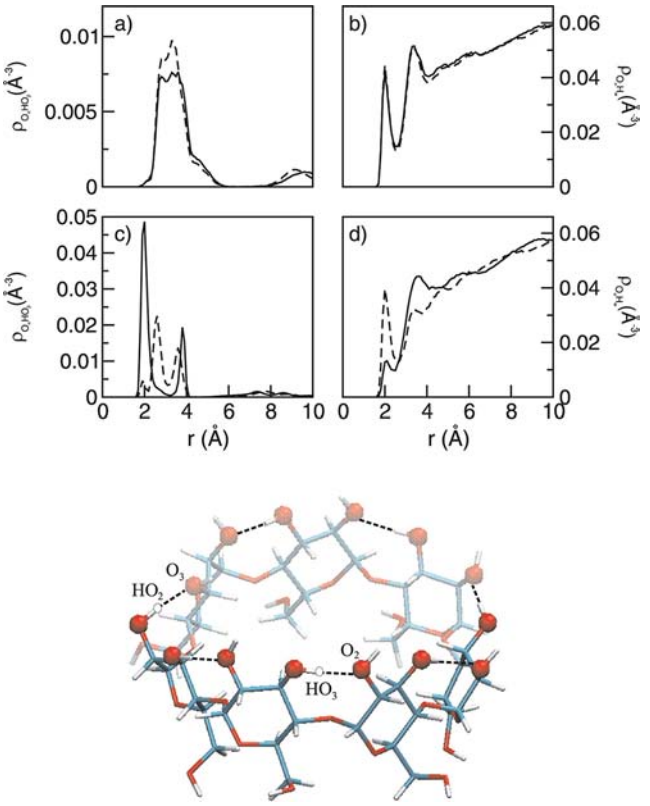

Figure 5. Upper panel: Radial density functions for $C_{12}mim^+$ encapsulation in a β-CD. (a, c) $\rho_{O_\alpha HO_\beta}$ for $\alpha = 2$, $\beta = 3$ (solid lines), or $\alpha = 3$, $\beta = 2$ (dashed lines); (b, d) $\rho_{O_\alpha H_w}$, for $\alpha = 2$ (solid lines) or $\alpha = 3$ (dashed lines). The upper (lower) graphs correspond to insertion pathways $\mathcal{A}$ ($\mathcal{B}$). Lower panel: Labeling scheme for the different atom types involved in intramolecular hydrogen bonds at the secondary rim of CD.

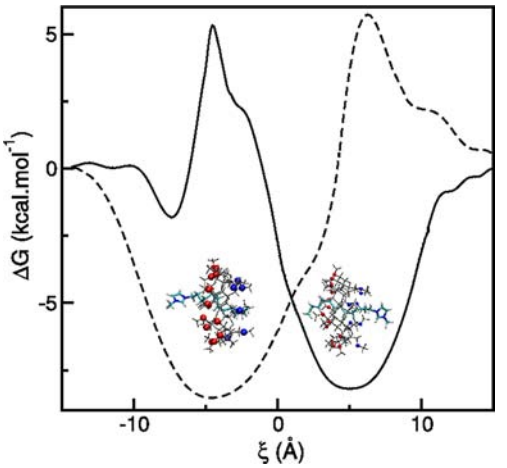

Figure 6. Gibbs free energy profiles for the inclusion of $C_{12}mim^+$ within a permethylated β-CD. The dashed and solid lines correspond to the $\mathcal{A}$ and $\mathcal{B}$ insertion pathways, respectively. Typical snapshots of the inclusion complexes at the minimum energy configurations for both insertion pathways are displayed.

the solvation structure of the cyclodextrin, despite the fact that the polar head lies sufficiently distant from the secondary rim. In pathway $\mathcal{A}$ these missing hydrogen bonds are compensated by an increment in the hydration of the secondary rim (see profiles for $\rho_{O_2H_w}$ and $\rho_{O_3H_w}$, depicted in Figure 5b). For the sake of comparison, similar correlation functions for pathway $\mathcal{B}$ are shown in Figure 5d. In the former case, both OH groups are fully solvated by water molecules, while in the latter, the solvation of these moieties is notably reduced (note the reduced magnitude of the peak of $\rho_{O_2H_w}$ at $r \sim 1.95$ Å). Incidentally, we mention that when this analysis is performed for the C_4mim^+–β-CD complex (not shown), the shape of the correlation function looks similar to the profile for the β-CD–water system, revealing that the presence of the shorter RTIL does not modify substantially the intramolecular hydrogen bond structure of the CD.

To carry on with our analysis, we investigated whether the perturbation in the solvation of the secondary rim of the CD was responsible for the difference between the minimum energy structures associated with both encapsulation pathways. To this end, we analyzed the free energy profile associated with the order parameter ξ for the encapsulation of $C_{12}mim^+$ in a permethylated β-CD (PMCD). Results are depicted in Figure 6. For both insertion pathways these profiles look almost perfectly symmetric, exhibiting similar stabilities. Furthermore, the magnitude of the global minimum is in good agreement with that of pathway $\mathcal{A}$ for the nonmethylated β-CD, where the intramolecular hydrogen bonds in the secondary rim were perturbed due to the presence of the encapsulated RTIL. In passing, note that the positions of the global minima and maxima are shifted compared with the system studied in Figure 3, most likely due to changes in the polarities of the rims.

To conclude our analysis, we provide a microscopic interpretation for the disruption of the intramolecular β-CD hydrogen bonds along the pathway $\mathcal{A}$. For this purpose it will be useful to focus on the time evolution of two parameters: (i) First, $d_{O_2-O_3}$, the average distance between oxygens belonging to adjacent glycosidic units in the CD. This parameter reflects the degree of deformation undergone by the CD, which, in turn, should favor or prevent the formation of intramolecular hydrogen bonds. In the upper panel in Figure 7 we show the time evolution of $d_{O_2-O_3}$ for the different insertion pathways. For pathway $\mathcal{A}$, $d_{O_2-O_3}$ fluctuates around ∼3.9 Å (see black line), while for pathway $\mathcal{B}$ the average distance is ∼1 Å smaller (see red line). (ii) The second parameter of interest is $|\cos\theta|$, defined as

$$|\cos\theta| = \frac{|Z_{IL} - Z_{CD}|}{|\mathbf{r}_{IL} - \mathbf{r}_{CD}|} \quad (12)$$

where $\mathbf{r}_{CD}$ and $\mathbf{r}_{IL}$ stand for the positions of the centers of mass of the β-CD and the RTIL imidazolium group, respectively. This magnitude provides an estimate of the degree of bending of the polar head with respect to its backbone.

The lower panel of Figure 7 depicts the time evolution of $|\cos\theta|$. It is clear that, for the $\mathcal{A}$ pathway, the fluctuation of this angle is larger (black lines) than that corresponding to the other orientation (red lines). Indeed, it can be seen that the glycosidic units of the β-CD that are closer to the bent RTIL head rotate almost ∼45° over the glycosidic bonds (not shown). From these observations it is possible to conclude that the larger fluctuations of the RTIL backbone along pathway $\mathcal{A}$ promote a stronger deformation of the secondary rim of CD and, consequently, prevent the formation of intramolecular hydrogen bonds.

DOI: 10.1021/acs.jpcb.5b00909
J. Phys. Chem. B XXXX, XXX, XXX–XXX

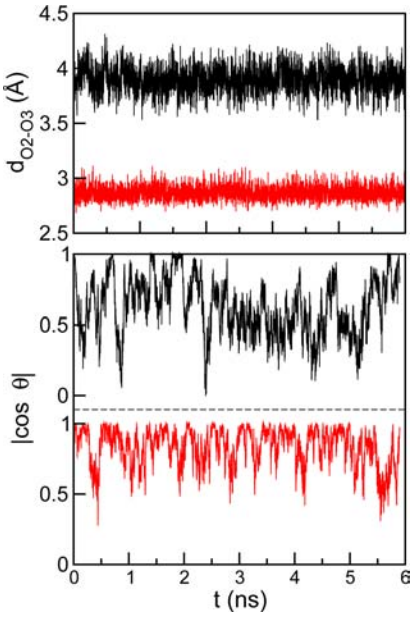

Figure 7. Time evolution of two relevant observables to explain the loss of intramolecular hydrogen bonds in $C_{12}mim^+$ encapsulation by pathway $\mathcal{A}$ (black lines) versus pathway $\mathcal{B}$ (red lines). Upper panel: $d_{O_2-O_3}$. Lower panel: |cos θ|.

5. CONCLUDING REMARKS

The MD results presented in this paper provide new insights into the microscopic characteristics of the individual encapsulation of two ionic liquids (differing in the lengths of their hydrophobic tails) within a β-CD. By means of an ABF scheme, we were able to obtain free energy profiles associated with the encapsulation processes for each RTIL, along two possible insertion pathways. We found that, for each pathway, there is only one minimum energy configuration for the $C_{12}mim^+$–β-CD complex. This structure is characterized by the hydrophobic RTIL tail embedded within the CD and the imidazolium head lying at an average distance of ∼11–12 Å from one of the rims. The arrangement in which the polar head lies closer to the primary rim (pathway $\mathcal{B}$) was found to be ∼50% more stable. The difference in the stability of the two complexes may be ascribed to the formation of intramolecular hydrogen bonds between adjacent glycosidic units in the secondary rim, which is only possible for pathway $\mathcal{B}$. Instead, when the insertion proceeds according to channel $\mathcal{A}$, the secondary rim suffers a deformation due to larger fluctuations of the alignment of the imidazolium head with respect to the z-axis, preventing the formation of these intramolecular hydrogen bonds.

On the other hand, the free energy associated with the encapsulation process of the C_4mim^+ shows two minima for each insertion pathway. For both channels, the most stable configurations correspond to an arrangement where the hydrophobic tail lies embedded within the β-CD, while the polar head lies close to one of the rims. The global minimum corresponds to the structure where the imidazolium lies close to the secondary rim. We examined a simplified model that incorporates the basic elements controlling the encapsulation channels. In doing so, we found that the latter difference can be simply ascribed to changes in the RTIL head–CD rim Coulombic couplings. Moreover, along each pathway, the shallower minima correspond to the scenarios where imidazolium interacts more strongly with one of the rims of the β-CD, while the hydrophobic tail remains surrounded by water molecules.

The obtained results suggest that hydrophobic interactions are the main responsible forces for the complexation process of RTILs in β-CD. Guest–host Coulombic interactions and hydrogen bond interactions could also play significant roles in the encapsulation process, and they are most influential on the characteristics and energetics of the system for imidazolium cations with shorter alkyl chains.

AUTHOR INFORMATION

Corresponding Author

*Tel.: 54-11-6772-7046. Fax: 54-11-6772-7121 E-mail: javier@speedy.cnea.gov.ar.

Notes

The authors declare no competing financial interest.

ACKNOWLEDGMENTS

R.S. thanks CONICET for a research fellowship. J.R. holds a research position at CONICET.

REFERENCES

(1) Larger cyclodextrins have also been reported; see, for instance: Larsen, K. L. Large Cyclodextrins. *J. Inclusion Phenom.* **2002**, *43*, 1–13.
(2) Astray, G.; Gonzalez-Barreiro, C.; Mejuto, J. C.; Rial-Otero, R.; Simal-Gándara, J. A Review on the Use of Cyclodextrins in Foods. *Food Hydrocolloids* **2009**, *23*, 1631–1640.
(3) Pinho, E.; Grootveld, M.; Soares, G.; Henriques, M. Cyclodextrins as Encapsulation Agents for Plant Bioactive Compounds. *Carbohydr. Polym.* **2014**, *101*, 121–135.
(4) Mellet, C. O.; Fernández, J. M. G.; Benito, J. M. Cyclodextrin-based Gene Delivery Systems. *Chem. Soc. Rev.* **2011**, *40*, 1586–1608.
(5) Loftsson, T.; Duchêne, D. Cyclodextrins and their Pharmaceutical Applications. *Int. J. Pharm.* **2007**, *329*, 1–11.
(6) Fraceto, L. F.; Grillo, R.; Sobarzo-Sánchez, E. Cyclodextrin Inclusion Complexes Loaded in Particles as Drug Carrier Systems. *Curr. Top. Med. Chem.* **2014**, *14*, 518–525.
(7) Van de Manakker, F.; Vermonden, T.; Van Nostrum, C. F.; Hennink, W. E. Cyclodextrin-based Polymeric Materials: Synthesis, Properties, and Pharmaceutical/Biomedical Applications. *Biomacromolecules* **2009**, *10*, 3157–3175.
(8) Li, J.; Loh, X. J. Cyclodextrin-based Supramolecular Architectures: Syntheses, Structures, and Applications for Drug and Gene Delivery. *Adv. Drug Delivery Rev.* **2008**, *60*, 1000–1017.
(9) Crini, G.; Morcellet, M. Synthesis and Applications of Adsorbents Containing Cyclodextrins. *J. Sep. Sci.* **2002**, *25*, 789–813.
(10) Welton, T. Room-Temperature Ionic Liquids. Solvents for Synthesis and Catalysis. *Chem. Rev.* **1999**, *99*, 2071–2084.
(11) Cui, Y.; Zhao, M.; Jiang, Z.; Xu, S.; Guo, X. Combined Use of Ionic Liquid and Hydroxypropyl-β-Cyclodextrin for the Enantioseparation of Ten Drugs by Capillary Electrophoresis. *Chirality* **2013**, *25*, 409–414.
(12) François, Y.; Varenne, A.; Juillerat, E.; Villemin, D.; Gareil, P. Evaluation of Chiral Ionic Liquids as Additives to Cyclodextrins for Enantiomeric Separations by Capillary Electrophoresis. *J. Chromatogr. A* **2007**, *1155*, 134–141.
(13) Wang, B.; He, J.; Bianchi, V.; Shamsi, S. A. Combined Use of Chiral Ionic Liquid and Cyclodextrin for MEKC: Part I. Simultaneous Enantioseparation of Anionic Profens. *Electrophoresis* **2009**, *30*, 2812–2819.
(14) Wang, B.; He, J.; Bianchi, V.; Shamsi, S. A. Combined Use of Chiral Ionic Liquid and CD for MEKC: Part II. Determination of Binding Constants. *Electrophoresis* **2009**, *30*, 2820–2828.
(15) Zhou, Z.; Li, X.; Chen, X.; Hao, X. Synthesis of Ionic Liquids Functionalized β-Cyclodextrin-bonded Chiral Stationary Phases and

DOI: 10.1021/acs.jpcb.5b00909
J. Phys. Chem. B XXXX, XXX, XXX–XXX

their Applications in High-Performance Liquid Chromatography. *Anal. Chim. Acta* **2010**, *678*, 208−214.
(16) Huang, K.; Zhang, X. T.; Armstrong, D. W. Ionic Cyclodextrins in Ionic Liquid Matrices as Chiral Stationary Phases for Gas Chromatography. *J. Chromatogr. A* **2010**, *1217*, 5261−5273.
(17) Amajjahe, S.; Chow, S.; Munteanu, M.; Ritter, H. Pseudopolyanions Based on Poly(NIPAAM-co-β-CyclodextrinMethacrylate) and Ionic Liquids. *Angew. Chem., Int. Ed.* **2008**, *47*, 3435−3437.
(18) Amajjahe, S.; Ritter, H. Supramolecular Controlled Pseudo-LCST Effects of Cyclodextrin-Complexed Poly(Ionic Liquids). *Macromolecules* **2008**, *41*, 3250−3253.
(19) Leclercq, L.; Schmitzer, A. R. Supramolecular Encapsulation of 1,3-bis(1-adamantyl)imidazolium Chloride by β-Cyclodextrins: Towards Inhibition of C(2)-H/D Exchange. *J. Phys. Org. Chem.* **2009**, *22*, 91−95.
(20) Gonsior, N.; Hetzer, M.; Kulicke, W. M.; Ritter, H. First Studies on the Influence of Methylated β-Cyclodextrin on the Rheological Behavior of 1-Ethyl-3-methyl Imidazolium Acetate. *J. Phys. Chem. B* **2010**, *114*, 12468−12472.
(21) Araki, J.; Ito, K. Recent Advances in the Preparation of Cyclodextrin-based Polyrotaxanes and Their Applications to Soft Materials. *Soft Matter* **2007**, *3*, 1456−1473.
(22) Shen, X.; Chen, Q.; Zhang, J.; Fu, P. Chapter 19. Supramolecular Structures in the Presence of Ionic Liquids. In *Ionic Liquids: Theory, Properties, New Approaches*; Kokorin, A., Ed.; InTech Europe: Rijeka, Croatia, 2011; pp 427−482.
(23) Gao, Y. A.; Li, Z. H.; Du, J. M.; Han, B. X.; Li, G. Z.; Hou, W. G.; Shen, D.; Zheng, L. Q.; Zhang, G. Y. Preparation and Characterization of Inclusion Complexes of β-Cyclodextrin with Ionic Liquid. *Chem.—Eur. J.* **2005**, *11*, 5875−5880.
(24) Gao, Y.; Zhao, X.; Dong, B.; Zheng, L.; Li, N.; Zhang, S. Inclusion Complexes of β-Cyclodextrin with Ionic Liquid Surfactants. *J. Phys. Chem. B* **2006**, *110*, 8576−8581.
(25) He, Y.; Chen, Q.; Xu, C.; Zhang, J.; Shen, X. Interaction between Ionic Liquids and β-Cyclodextrin: A Discussion of Association Pattern. *J. Phys. Chem. B* **2009**, *113*, 231−238.
(26) Zhang, J.; Shen, X. Multiple Equilibria Interaction Pattern between the Ionic Liquids $C_n$mimPF_6 and β-Cyclodextrin in Aqueous Solutions. *J. Phys. Chem. B* **2011**, *115*, 11852−11861.
(27) Zhang, J.; Shi, J.; Shen, X. Further Understanding of the Multiple Equilibria Interaction Pattern between Ionic Liquid and β-Cyclodextrin. *J. Inclusion Phenom. Macrocyclic Chem.* **2014**, *79*, 319−327.
(28) Franćois, Y.; Varenne, A.; Sirieix-Plenet, J.; Gareil, P. Determination of Aqueous Inclusion Complexation Constants and Stoichiometry of Alkyl(methyl)-methylimidazolium-based Ionic Liquid Cations and Neutral Cyclodextrins by Affinity Capillary Electrophoresis. *J. Sep. Sci.* **2007**, *30*, 751−760.
(29) Ondo, D.; Tkadlecová, M.; Dohnal, V.; Rak, J.; Kvíčala, J.; Lehmann, J. K.; Heintz, A.; Ignatiev, N. Interaction of Ionic Liquids Ions with Natural Cyclodextrins. *J. Phys. Chem. B* **2011**, *115*, 10285−10297.
(30) Lipkowitz, K. Applications of Computational Chemistry to the Study of Cyclodextrins. *Chem. Rev.* **1998**, *98*, 1829−1873.
(31) Phillips, J. C.; Braun, R.; Wang, W.; Gumbart, J.; Tajkhorshid, E.; Villa, E.; Chipot, C.; Skeel, R. D.; Kale, L.; Schulten, K. Scalable Molecular Dynamics with NAMD. *J. Comput. Chem.* **2005**, *26*, 1781−1802.
(32) MacKerell, A. D., Jr.; Bashford, D.; Bellott, M.; Dunbrack, R. L., Jr.; Evanseck, J. D.; Field, M. J.; Fischer, S.; Gao, J.; Guo, H.; Ha, S.; et al. All-Atom Empirical Potential for Molecular Modeling and Dynamics Studies of Proteins. *J. Phys. Chem. B* **1998**, *102*, 3586−3616.
(33) Liu, Z.; Huan, S.; Wang, W. A Refined Force Field for Molecular Simulation of Imidazolium-Based Ionic Liquids. *J. Phys. Chem. B* **2004**, *108*, 12978−12989.
(34) Jorgensen, W. L.; Chandrasekhar, J.; Madura, J.; Impey, R. W.; Klein, M. L. Comparison of Simple Potential Functions for Simulating Liquid Water. *J. Chem. Phys.* **1983**, *79*, 926−935.
(35) Rodriguez, J.; Elola, M. D. Encapsulation of Small Ionic Molecules within α-Cyclodextrins. *J. Phys. Chem. B* **2009**, *113*, 1423−1428.
(36) Rodriguez, J.; Semino, R.; Laria, D. Building up Nanotubes: Docking of "Janus" Cyclodextrins in Solution. *J. Phys. Chem. B* **2009**, *113*, 1241−1244.
(37) Rodriguez, J.; Elola, M. D.; Laria, D. Ionic Liquid Aqueous Solutions under Nanoconfinement. *J. Phys. Chem. C* **2012**, *116*, 5394−5400.
(38) Elola, M. D.; Rodriguez, J. Structure and Dynamics of Nonionic Surfactants Adsorbed at Vacuum/Ionic Liquid Interfaces. *Langmuir* **2013**, *29*, 13379−13387.
(39) Betzel, C.; Saenger, W.; Hingerty, B. E.; Brown, G. Topography of cyclodextrin inclusion complexes, part 20. Circular and flip-flop hydrogen bonding in β-cyclodextrin undecahydrate: a neutron diffraction study. *J. Am. Chem. Soc.* **1984**, *106*, 7545−7557.
(40) Hwang, H.; Schatz, G. C.; Ratner, M. A. Steered Molecular Dynamics Studies of the Potential of Mean Force of a Na^+ or K^+ Ion in a Cyclic Peptide Nanotube. *J. Phys. Chem. B* **2006**, *110*, 26448−26460.
(41) Darve, E.; Pohorille, A. Calculating Free Energies Using Average Force. *J. Chem. Phys.* **2001**, *115*, 9169−9183.
(42) Hénin, J.; Chipot, C. Overcoming Free Energy Barriers Using Unconstrained Molecular Dynamics Simulations. *J. Chem. Phys.* **2004**, *121*, 2904−2914.
(43) Rodriguez-Gomez, D.; Darve, E.; Pohorille, A. Assessing the Efficiency of Free Energy Calculation Methods. *J. Chem. Phys.* **2004**, *120*, 3563−3578.
(44) Cai, W.; Sun, T.; Liu, P.; Chipot, C.; Shao, X. Inclusion Mechanism of Steroid Drugs into β-Cyclodextrins. Insights from Free Energy Calculations. *J. Phys. Chem. B* **2009**, *113*, 7836−7843.
(45) Yu, Y.; Chipot, C.; Sun, T.; Shao, X. Spatial Arrangement of α-Cyclodextrins in a Rotaxane. Insights from Free-Energy Calculations. *J. Phys. Chem. B* **2008**, *112*, 5268−5271.
(46) Yu, Y.; Chipot, C.; Cai, W.; Shao, X. Molecular Dynamics Study of the Inclusion of Cholesterol into Cyclodextrins. *J. Phys. Chem. B* **2006**, *110*, 6372−6378.
(47) He, J.; Chipot, C. J.; Shao, X.; Cai, W. Cyclodextrin-Mediated Recruitment and Delivery of Amphotericin B. *J. Phys. Chem. C* **2013**, *177*, 11750−11756.
(48) See note added in proof: Dang, L. X.; Kollman, P. A. Free Energy of Association of the 18-Crown-6:K^+ Complex inWater: A Molecular Dynamics Simulation. *J. Am. Chem. Soc.* **1990**, *112*, 5716−5720.
(49) Yoshimura, Y.; Takekiyo, T.; Imai, Y.; Abe, H. High Pressure Phase Behavior of Two Imidazolium-Based Ionic Liquids, [bmim][BF4] and [bmim][PF6]. In *Ionic Liquids—Classes and Properties*; Handy, S. T., Ed.; InTech Europe.: Rijeka, Croatia, 2011; pp 171−186.
(50) Uematsu, M.; Franck, E. U. Static Dielectric Constant of Water and Steam. *J. Phys. Chem. Ref. Data* **1980**, *9*, 1291−1306.
(51) Chowdhary, J.; Ladanyi, B. M. Hydrogen Bond Dynamics at the Water/Hydrocarbon Interface. *J. Phys. Chem. B* **113**, *13*, 4045−4053.

DOI: 10.1021/acs.jpcb.5b00909
J. Phys. Chem. B XXXX, XXX, XXX−XXX